

Solution Structure of the Core NFATC1/DNA Complex

Pei Zhou,*[§] Li Jing Sun,*[§] Volker Dötsch,[†]
Gerhard Wagner,[†] and Gregory L. Verdine*[‡]

*Department of Chemistry and Chemical Biology
Harvard University
Cambridge, Massachusetts 02138

[†]Department of Biological Chemistry and
Molecular Pharmacology
Harvard Medical School
Boston, Massachusetts 02115

Summary

The nuclear factor of the activated T cell (NFAT) family of transcription factors regulates cytokine gene expression by binding to the promoter/enhancer regions of antigen-responsive genes, usually in cooperation with heterologous DNA-binding partners. Here we report the solution structure of the binary complex formed between the core DNA-binding domain of human NFATC1 and the ARRE2 DNA site from the interleukin-2 promoter. The structure reveals that DNA binding induces the folding of key structural elements that are required for both sequence-specific recognition and the establishment of cooperative protein-protein contacts. The orientation of the NFAT DNA-binding domain observed in the binary NFATC1-DBD*/DNA complex is distinct from that seen in the ternary NFATC2/AP-1/DNA complex, suggesting that the domain reorients upon formation of a cooperative transcriptional complex.

Introduction

Transcription factors of the NFAT family control the activation of genes encoding cytokines and their receptors in response to antigenic stimulation of immune cells (Crabtree and Clipstone, 1994; Rao et al., 1997). Localized in the cytoplasm of resting cells, NFAT translocates to the nucleus upon dephosphorylation by the Ca²⁺-activated Ser/Thr phosphatase calcineurin (Crabtree and Clipstone, 1994; Rao et al., 1997). The clinically important immunosuppressive agents FK506 and cyclosporin A block nuclear translocation of NFAT by directly inhibiting the phosphatase activity of calcineurin (Liu et al., 1991). The pronounced toxicity of these agents has created impetus for the development of new drugs that suppress T cell activation through inhibition of novel protein targets, foremost among which is NFAT.

In most instances, NFAT activates gene transcription only in cooperation with a heterologous transcription factor, which is induced by a p21^{ras}-dependent signaling pathway (Flanagan et al., 1991; Woodrow et al., 1993); this partner is most likely a basic-leucine zipper (bZIP)

protein related or identical to members of the AP-1 family (Jain et al., 1992). The Ca²⁺-dependent and p21^{ras}-dependent signaling pathways that emanate in parallel from the T cell receptor (TCR) are thus reintegrated through NFAT-mediated assembly of a transcriptional complex on lymphokine gene promoters. NFAT and its transcriptional partner bind to composite recognition elements containing closely juxtaposed binding sites for each of the two proteins (Rao, 1994; Chen et al., 1995). NFAT and AP-1 can be chemically cross-linked, but only in the presence of a composite recognition element, suggesting the two cooperate on DNA through the establishment of weak protein-protein contacts (Chen et al., 1995). Consistent with this notion, NFAT cooperates with only one of the two DNA-bound orientational isomers of AP-1 (Chen et al., 1995), and mutations have been found in both NFAT and AP-1 that impair their cooperation but have no effect on DNA binding by either protein alone (Peterson et al., 1996; Sun et al., 1997).

The NFAT family consists of at least four known genes, each of which exhibits a characteristic pattern of cell-type specificity. NFATC1 and NFATC2 appear to be the major forms in developed T cells, with the constitutive NFATC2 (also known as NFATp) predominating in resting T cells, and the NFATC1 form (also known as NFATc) being induced to significant levels upon stimulation of Ca²⁺-dependent signaling (Crabtree and Clipstone, 1994). Homozygous targeted disruption of the *NFATC2* gene in mice gives rise to a T cell hyperproliferative phenotype (Hodge et al., 1996; Xanthoudakis et al., 1996); on the other hand, disruption of *NFATC1* results in T cell depletion, in addition to defects in cardiac valve development (G. R. Crabtree, personal communication).

The protein sequences of NFAT family members contain two regions of significant homology, each of which corresponds to a distinct functional domain (Rao et al., 1997). The N-terminal domain controls Ca²⁺-dependent subcellular localization (Luo et al., 1996; Shibasaki et al., 1996; Beals et al., 1997), whereas the C-terminal domain binds DNA sequence-specifically and cooperates with AP-1 in vitro (Rao, 1994; Wolfe, 1996). A 20 kDa fragment of the NFATC1 C-terminal domain comprising residues 416–591 (NFATC1-DBD) binds DNA sequence-specifically (Wolfe, 1996); a related fragment of NFATC2 has been found to behave similarly (Jain et al., 1995). Importantly, even though NFATC1-DBD binds DNA more weakly than the full C-terminal domain, the two proteins show practically identical affinities for DNA in the presence of AP-1 (Wolfe, 1996). Consistent with this observation, NFAT-DBD cooperatively activates the distal antigen receptor response element of the IL-2 enhancer (ARRE2) in transfected cells (S. N. Ho and G. R. Crabtree, personal communication). The solution structure of NFATC1-DBD (Wolfe et al., 1997) revealed a common overall fold with the DNA-binding domain of Rel family proteins, as represented by NF- κ B p50 (Ghosh et al., 1995; Müller et al., 1995). However, the NFAT-DBD and p50 structures exhibited significant local differences in regions that participate in intermolecular contacts, indicating that the two classes of Rel protein employ distinct

[‡]To whom correspondence should be addressed.

[§]These authors contributed equally to this work.

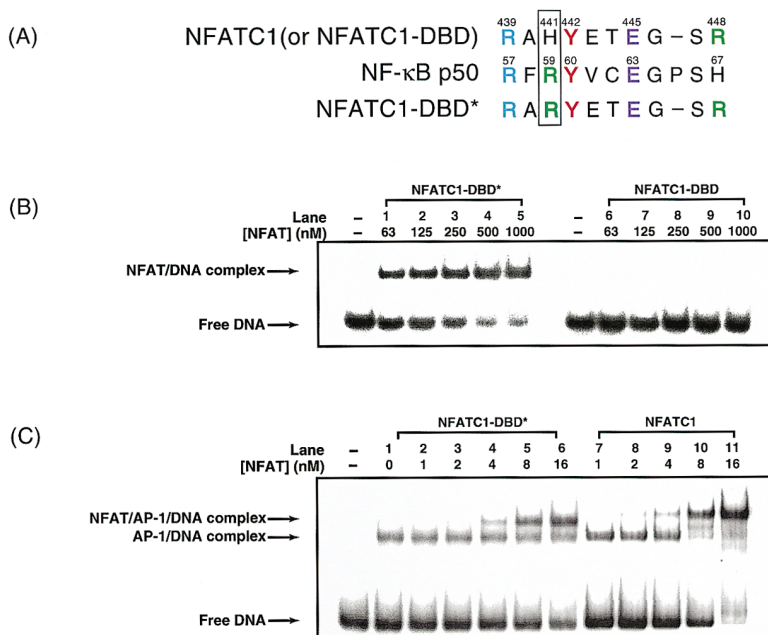


Figure 1. A Point Mutation in the DNA-Binding Loop of NFATC1-DBD Increases the Affinity for DNA

(A) Comparison of the sequences of the DNA-binding loops of NFATC1 (same as NFATC1-DBD), NF-κB p50, and NFATC1-DBD*. Box indicates the position (441 in NFATC1 and 59 in NF-κB-p50) of the gain-of-function mutation.

(B) Electrophoretic mobility shift assay (EMSA) demonstrating the effect of the His-441 to Arg mutation on the affinity for ARRE2. NFATC1-DBD is the wild-type (His-441) form of the core DNA-binding domain; NFATC1-DBD* is the gain-of-function mutant form (Arg-441). Protein concentrations were as indicated; the DNA concentration was held constant at 100 pM.

(C) EMSA assay demonstrating the comparable affinities of NFATC1 and NFATC1-DBD* for DNA in the presence of the AP-1 bZIP domain. The concentrations of NFATC1-DBD* and NFATC1 C-terminal domain were as indicated; the concentration of the AP-1 bZIP domain was held constant at 200 nM, and the DNA concentration was 100 pM.

strategies for recognition of DNA and interaction with other proteins.

Here we report the solution structure of the binary complex formed between the minimal DNA recognition domain of human NFATC1 and a 12 bp oligonucleotide duplex containing the ARRE2 sequence. This structure provides insight into the molecular basis for sequence-specific DNA recognition and signal integration by NFAT, reveals the important role of induced fit processes in NFAT function, and represents a starting point for structure-based discovery of novel immunosuppressive agents that target NFATC1 directly.

Results and Discussion

A Gain-of-Function Mutation in NFATC1-DBD

In preliminary efforts to determine the DNA-bound structure of NFATC1-DBD, we performed two-dimensional (2D) ^1H - ^{15}N heteronuclear single quantum coherence (HSQC) experiments on ^{15}N -labeled NFATC1-DBD mixed with an equimolar amount of an ARRE2 oligonucleotide. Under all conditions tested, the observed spectra contained substantially fewer cross-peaks than expected. The wild-type NFATC1-DBD/ARRE2 complex was therefore deemed unsuitable for detailed NMR structural analysis. We reasoned that these effects might be due to the relatively weak DNA-binding affinity of NFATC1-DBD, which suggested that the quality of the spectra might be improved by modifying either the protein or DNA so as to increase their mutual affinity. In comparing the sequences of the DNA-binding loops of NF-κB p50 and NFATC1, we noted that one DNA contact residue in p50 (Arg-59) is replaced by a His residue (His-441) in NFATC1 (Figure 1A). We therefore mutated His-441 in NFATC1-DBD to Arg (H441R mutation) and measured the affinity of the resulting protein (NFATC1-DBD*) for DNA, both alone and in the presence of AP-1. Remarkably, NFATC1-DBD* bound ARRE2 much more strongly

than the wild-type NFATC1-DBD fragment (Figure 1B). Furthermore, NFATC1-DBD* formed a cooperative complex with AP-1 that is roughly comparable in stability to that formed with the full NFATC1 C-terminal domain (Figure 1C).

Structure Determination

The binary complex formed between ^{15}N -labeled NFATC1-DBD* and a 12 bp oligonucleotide containing the core NFAT recognition site from murine ARRE2 exhibited excellent ^1H - ^{15}N HSQC spectra (data not shown). The three-dimensional structure of the NFATC1-DBD*/12-mer complex was determined through a series of 2D and 3D NMR experiments. Because of the relatively large size of the NFAT-DBD*/DNA complex, we employed isotopic labeling to enable the differentiation of inter- from intramolecular contacts. Specifically, (1) 3D ^{15}N -separated NOESY measurements were performed on samples containing perdeuterated, ^{15}N -labeled protein to identify intermolecular NOEs between observable N-H protons of NFAT-DBD* and protons on DNA; (2) 2D ^1H - ^1H homonuclear NOESY measurements were performed in D_2O and in H_2O with a perdeuterated protein sample containing fully protonated Tyr and Phe residues, to characterize the contacts between Tyr 442 and DNA; (3) 3D ^{15}N -separated NOESY experiments in H_2O and 3D ^{13}C -separated NOESY measurements in D_2O were both carried out on a sample of perdeuterated NFAT-DBD* containing fully ^{15}N , ^{13}C , ^1H -labeled Arg residues, to assign interfacial contacts between Arg residues and DNA. Site-specific deuteration of the DNA was also carried out to confirm NOE contacts between the protein and minor groove adenines of the DNA. Based on the NMR data thus obtained, we used a torsion angle dynamics (Güntert et al., 1997)/simulated annealing (Brünger, 1992) procedure to calculate the family of 18 final structures presented in Figure 2 (statistics shown in Table 1).

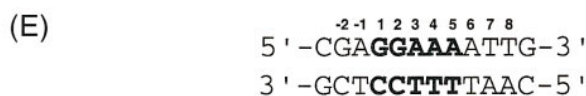
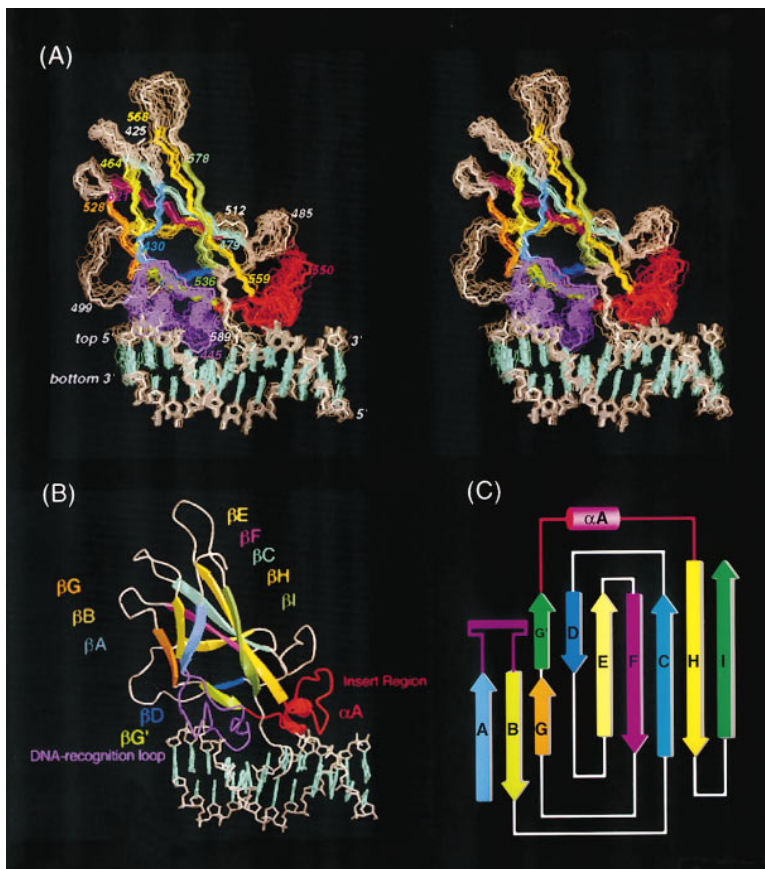


Figure 2. Solution Structure of NFATC1-DBD* Bound to a Duplex 12-mer Oligonucleotide

(A) Backbone (N,C α ,C') overlay of 18 calculated structures of the NFATC1-DBD*/12-mer complex, with the structure that possesses the closest fit to the average highlighted. The core domain consists of residues 425–590; residues 416–424 and 591, which are highly disordered, are not shown. Designations of top and bottom strand refer to the respective positions in (E).

(B) MOLSCRIPT representation of the NFATC1-DBD* structure, viewed from the same perspective as in (A).

(C) Topological representation of secondary structure elements in the complex.

(D) Sequence alignment of NFATC1, NFATC2, and NF- κ B p50 in the region of the core DNA-binding domain. Bold letters denote conserved residues. Italic numbering below all three sequences corresponds to that for the respective full-length proteins. Red asterisks, residues that make sequence-specific contacts to DNA; blue, phosphate contact residues; boxed yellow residue, position at which a gain-of-function His to Arg mutation was introduced into NFATC1-DBD to generate NFATC1-DBD*. The italicized MK in the sequence of NFATC1-DBD* denotes amino acids added for purposes of overexpression, which are not present in NFATC1 itself. The color scheme for the individual secondary structure elements is matched in (A)–(D).

(E) Sequence of the duplex 12-mer used in this study. The hexaethyleneglycol linker located between the 3'-end of the top strand and the 5'-end of the bottom strand is not shown explicitly (also not shown in [A] and [B]).

Table 1. Structural Statistics for NFATC1-DBD*/DNA Complex

Protein		
Amino acids residues sequentially assigned (nonproline)		162 of 167
Effective distance constraints		1050
Intraresidue		236
Sequential ($ i - j = 1$)		374
Medium-range ($ i - j \leq 4$)		86
Long-range ($ i - j \geq 5$)		272
H bonds		82
Dihedral angle constraints		363
DNA		
Effective distance constraints		276
Intraresidue		146
Sequential		131
Interstrand		1
H bond		58
Protein-DNA interface		
Effective distance constraints		56
Distance constraint violations > 0.2 Å (per structure)		1.81 ± 2.07
Dihedral constraint violations > 3.0° (per structure)		1.44 ± 0.96
X-PLOR potential energy (E_{LJ} , Kcal/mol, avg. per structure)		-501 ± 28.9
R.m.s.d. to the mean for backbone heavy atoms of all β strands (residues 428-432, 460-464, 472-479, 493-495, 506-510, 515-521, 528-538, 559-568, 578-583)		0.62 ± 0.07
R.m.s.d. to the mean for heavy atoms of all β strands (residues 428-432, 460-464, 472-479, 493-495, 506-510, 515-521, 528-538, 559-568, 578-583)		1.20 ± 0.14
R.m.s.d. to the mean for backbone heavy atoms (residues 425-590)		1.14 ± 0.11
R.m.s.d. to the mean for heavy atoms (residues 425-590)		1.58 ± 0.10
R.m.s.d. to the mean for DNA heavy atoms (superposition of all DNA heavy atoms)		0.83 ± 0.21
R.m.s.d. to the mean for protein + DNA heavy atoms (superposition of all β strand heavy atoms and DNA heavy atoms)		1.20 ± 0.16
Ramachandran plot ^a		
	<u>Residues 425-590</u>	<u>Secondary Structures</u>
Most favorable region	60.4%	83.7%
Additionally allowed region	38.9%	14.0%
Generously allowed region	0.7%	2.3%
Disallowed region	0.0%	0.0%

^a Laskowski et al., 1996.

Comparison of DNA-Bound NFATC1-DBD* with the Unbound Protein

The overall fold of DNA-bound NFATC1-DBD* is very similar to that of unliganded NFATC1-DBD (Wolfe et al., 1997), comprising a ten-stranded antiparallel β -barrel (Figure 2), which is structurally related to s-type domains of the immunoglobulin (Ig) superfamily (Bork et al., 1994). The two primary sheets (β IHFCE and β ABG) that form the core of the β -barrel lie remote from the DNA interface and are almost completely unaffected by being bound to DNA. The third sheet (β DG'), which does not itself contact DNA directly but adjoins and abuts multiple segments that do, is also very similar in the free protein and binary complex. The most radical changes that occur upon binding to DNA involve two large surface loops. The β A- β B loop, which is only partially ordered in the unliganded protein (Wolfe et al., 1997), adopts a well-defined conformation in the binary complex. The β G'- β H loop, which is devoid of secondary structure in the absence of DNA (Wolfe et al., 1997), is folded in the binary complex and contains a short α helix (α A, Figures 2A and 2B). Binding of NFATC1-DBD* to DNA is accompanied by a 7.4% reduction in the overall solvent-accessible surface of the protein, corresponding to a contact surface area of 726 Å². The DNA in the NFATC1-DBD*/

12-mer complex is unbound and otherwise exhibits typical features of a B-form duplex, with the exception of modest minor groove compression at positions 4-6.

Contacts between NFATC1-DBD* and DNA

NFATC1-DBD* utilizes a combination of direct and indirect readout mechanisms involving both major and minor groove contacts to achieve DNA sequence specificity (Figures 3A-3C). The 5'-end of the recognition site (GAGGAAAA) is recognized mainly through major groove contacts made by residues of the DNA recognition loop (β A- β B loop). Several of these key contacts are very similar to those made by the homologous DNA recognition loop of NF- κ B p50 (Ghosh et al., 1995; Müller et al., 1995) (Figure 3C). The side chain guanidinium groups of Arg-441 and Arg-439 are positioned to hydrogen bond to G1 and G2, respectively, and are buttressed by the carboxylate of Glu-445 (Figure 3B). The side chain of Tyr-442 is brought close to T3' and T4' through a hydrophobic contact between the phenyl ring and the T3' methyl group, and a hydrogen bond between the hydroxyl and the DNA backbone phosphate located between T4' and T5' (T4'pT5'). The existence of this hydrogen bond is clearly evidenced by the direct observation

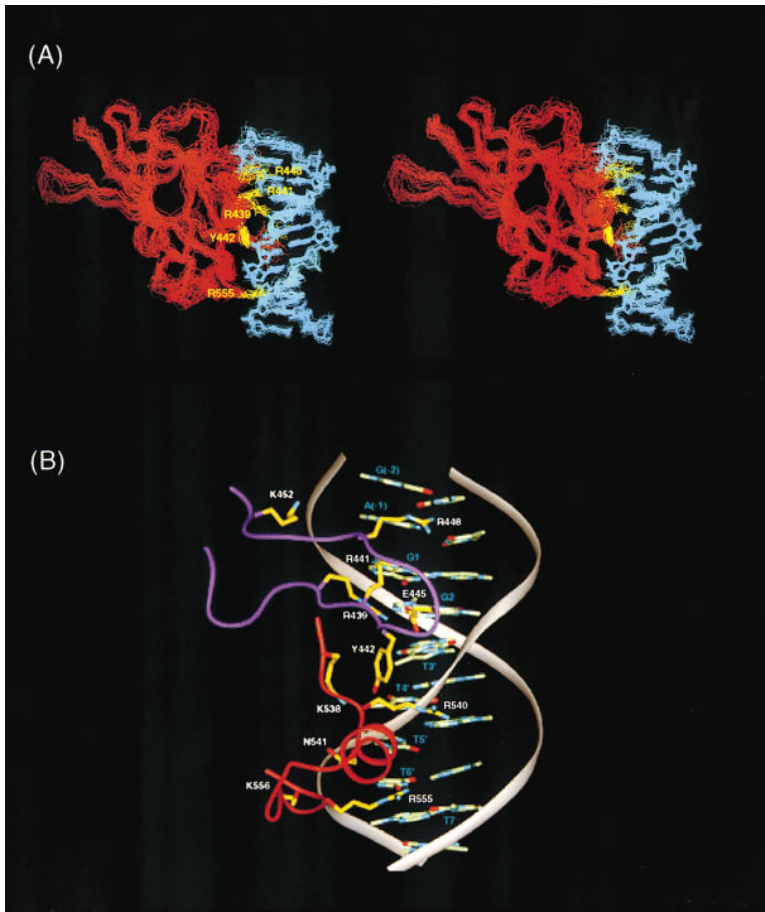


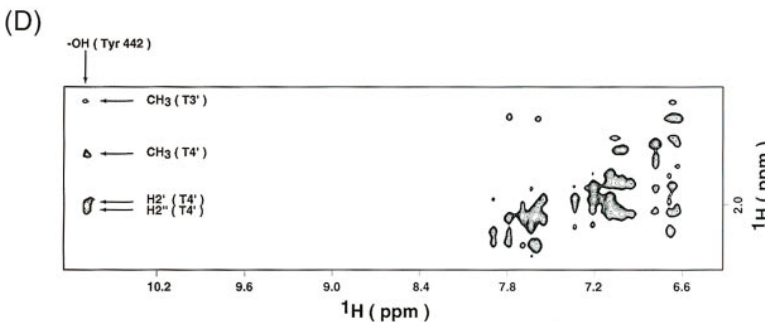
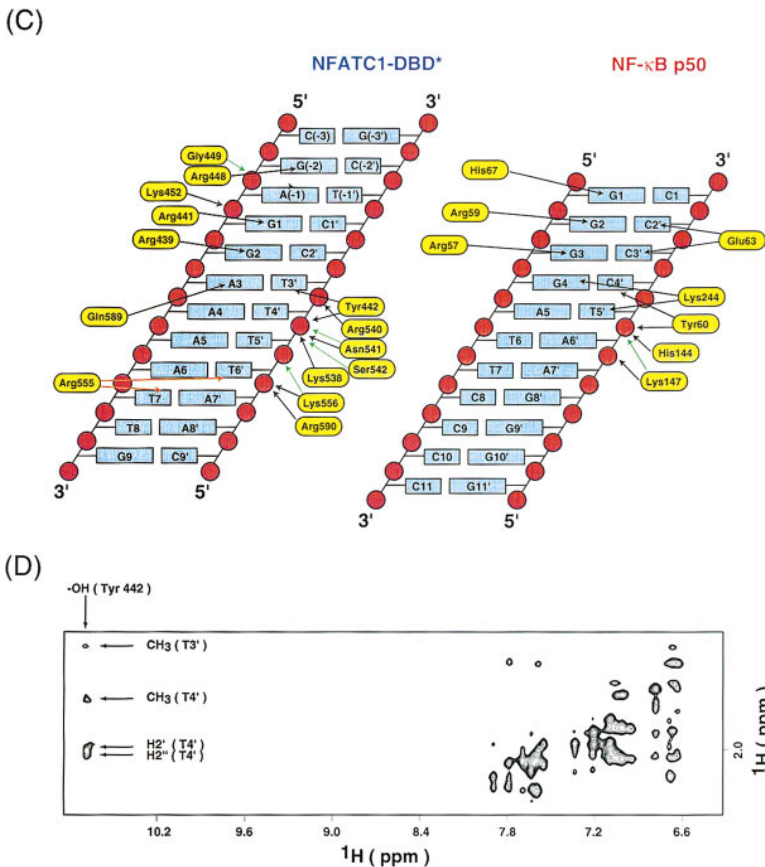
Figure 3. Sequence-Specific Contacts in the NFATC1-DBD*/12-mer Interface

(A) Protein–DNA interface in the family of 18 final structures. Blue, DNA; red, protein backbone trace; yellow, side chains that make sequence-specific contacts to DNA. Side chain of Gln-589 is concealed by the DNA in this view and hence not labeled.

(B) Ribbon trace of the DNA backbone (gray) and main DNA-contact elements of NFATC1-DBD*: DNA recognition loop (magenta) and insert region (red). The bases of the 12-mer are shown explicitly (C atoms, light green; N, blue; O, red), as are amino acid side chains that contact DNA directly (C atoms, yellow; N, blue; O, red). The C-terminal extended peptide (residues 585–591) is not shown.

(C) Schematic summary of interfacial contacts. DNA bases are depicted as light blue boxes, and backbone phosphates as red spheres. Black arrows represent major groove contacts to DNA bases; orange, minor groove contacts; green, backbone phosphate contacts.

(D) Section of a 2D homonuclear ^1H - ^1H NOESY spectrum of a binary complex formed using a perdeuterated protein sample, recorded in H_2O ($\tau = 80$ ms). Vertical arrow denotes the downfield-shifted resonance of the Tyr 442 hydroxyl group. Horizontal arrows denote protons in DNA that exhibit NOE cross-peaks to the Tyr 442 hydroxyl.



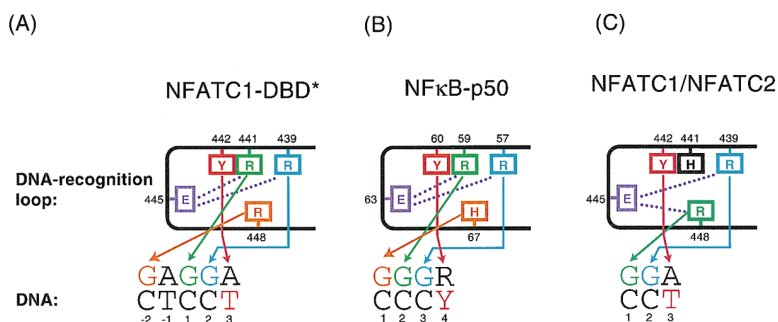


Figure 4. Comparison of the DNA Contacts Made by the DNA-Recognition Loops of Different Rel Proteins

(A) NFATC1-DBD*, (B) NF- κ B p50, and (C) NFATC1/NFATC2. Arrows denote contact pairs between protein residues and their interacting bases and are color matched. Bridging hydrogen bonds between a key conserved residue Glu (Glu-445 in NFATC1 and Glu-63 in NF- κ B-p50) are indicated by dotted lines.

of the Tyr-442 hydroxyl proton (10.68 ppm) and its multiple NOE cross-peaks to protons of T3' and T4' (Figure 3D). The phenyl ring contact has been independently confirmed by specific photo-cross-linking of Tyr-442 to a DNA probe containing 5-iododeoxyuridine in place of T3' (Wolfe et al., 1997). At the extreme 5'-end of the site, G(-2) is recognized through an interaction with Arg-448 (Figures 3A and 3B). The DNA recognition loop of NFATC1-DBD* appears to make two more contacts to the DNA backbone, one between Gly-449 and A(-1)pG (-2) and the other between Lys-452 and G1pA(-1) (Figure 3C). In addition to this ensemble of contacts made by the DNA recognition loop, one further sequence-specific contact may be contributed by an extended peptide stretch at the C-terminal end of NFATC1-DBD*. This stretch, most clearly visible in Figure 2B, is anchored in close proximity to bases of the major groove through a phosphate contact between Arg 590 and T6'pT7'. As a result, the side chain of Gln-589 is brought within reach of A3. A corresponding polypeptide stretch at the C-terminal end of the NF- κ B p50 DNA-binding domain interacts with DNA in a remarkably similar way but makes a Lys-G (p50: Lys-244-G4) rather than Gln-A (NFATC1-DBD*: Gln-589-A3) contact (Figure 3C).

Positions 4 and 5 in the poly(A) stretch of the NFAT site (GAGGAAA) are both highly conserved among known NFAT sites (Rao et al., 1997) and are selected at a high frequency in PCR site selection experiments using NFATC2 (C.D. Vaughan and G.L.V., unpublished data). The basis for such exquisite sequence specificity at these positions is not obvious from the structural data alone. No residue of NFATC1-DBD* is close enough to base pair 4 to make a sequence-specific interaction. Although the side chains of Ser-588 and Arg-590 are in the vicinity of T5', they do not appear to lie within optimal contact distance. Even if side chains of the protein do contact T5', these interactions do not appear to contribute to sequence specificity: switching base pairs 5 and 4 from A-T to I-C, which drastically alters major groove functionality but leaves minor groove functionality unperturbed, has little if any effect on the strength of NFATC1-DNA interactions (Wolfe et al., 1997). Taken together, these data suggest that NFATC1 (and NFATC2) recognizes A4 and A5 by sensing the sequence-dependent deformability of the poly(A) stretch, a mechanism known as "indirect readout." Consistent with this notion, the minor groove width of the 12-mer is compressed by greater than 1Å in this region of the binary complex (T4'04' \leftrightarrow A604' = 5.4 ± 0.4 Å; average B-DNA = 6.8 Å).

Finally, a residue of the insert region, Arg-555, projects

its side chain into the minor groove at the extreme 3'-end of the site to contact T6' and T7. The existence of this minor groove contact was established by the observation of an NOE cross-peak between the H ϵ of Arg-555 and H2 of A6, and confirmed by site-specific deuteration at C2 of A6, which resulted in loss of the assigned NOE cross-peak (data not shown). These sequence-specific contacts to the 3'-end of the site provide a basis for understanding the greater binding affinity of NFAT for murine versus human ARRE2, which differ at base pairs 7 and 8 (TT versus AC, respectively) (Jain et al., 1993; Hoey et al., 1995).

Structural Basis for the Gain-of-Function by the H441R Mutation

The gain of DNA-binding affinity associated with the H441R mutation in NFATC1-DBD* can be rationalized on the basis of the NMR complex structure. The introduced residue, Arg-441, contacts G1, while Arg-448 contacts G(-2) (Figure 4A). NFAT therefore uses the Arg residue at position 441 in much the same way as p50 uses the equivalent residue (Arg-59) in its DNA-binding loop (Figure 4B). It seems likely that wild-type NFATC1 uses position 441 differently, because the side chain of His-441 would be too short to contact G1 directly. However, as pointed out earlier (Wolfe et al., 1997), simple side chain rotations are all that would be required to swivel the Arg-448 side chain in to reach and contact G1, provided that His-441 swiveled out of the way (Figure 4C; refer also to Figure 3A); this could be accomplished with little or no alteration of the backbone conformation of the DNA recognition loop. Consistent with this notion, the Arg contact arrangement shown in Figure 4C is observed in the crystallographic structure of the ternary NFATC2/AP-1/DNA complex (Chen et al., 1998). All other factors thus being equal, it stands to reason that the additional Arg contacts made by NFATC1-DBD* should increase the affinity of the protein-DNA interaction relative to that of NFATC1-DBD. It is worth noting that NFATC1-DBD* and NFATC1-DBD both possess an Arg residue at position 448, and yet these two proteins use Arg-448 to make different contacts. Just as changes in a single nearby amino acid can cause Arg-448 to switch its DNA contact partner, so might changes in the DNA sequence cause similar switching. This raises the possibility that NFAT family members may be capable of switching between the two recognition modes, in a way that depends on the DNA sequence.

Induced Folding of DNA Contact Segments in NFATC1-DBD*

The DNA recognition elements of many transcription factors are disordered in the absence of DNA and undergo an induced folding transition upon interaction with DNA (Spolar and Record, 1994). Such behavior appears to be especially common among transcription factors that contain predominantly α -helical DNA recognition domains, such as members of the bZIP (Patel et al., 1990; Weiss et al., 1990) and basic helix-loop-helix (Ferre-D'Amare et al., 1993; Fisher et al., 1993) families. Even though the core DNA recognition domain of NFATC1 comprises predominantly β structure, the structure presented here reveals that it, too, undergoes an induced folding transition upon interaction with DNA. Specifically, NMR relaxation measurements on unliganded NFAT-DBD revealed that the Ig domain adopts a well-defined three-dimensional structure, with the exception of the β A-B and β G'-H loops, which are disordered (Wolfe et al., 1997). In the binary solution structure, both of these loops become ordered upon interaction with DNA, and indeed, both contribute directly to the DNA-contact interface (Figure 5A, compare top left and right). Especially striking is the structural transition of the insert region from a completely disordered loop to a compact module containing an α helix (α A). This helix appears to be stabilized directly through a hydrogen-bonding interaction between two of its N-terminal amide protons (Asn-541 and Ser-542) and a DNA backbone phosphate (T5'pT6'), and the overall helix is aligned so as to permit a favorable interaction of its helix dipole with DNA (readily visible in Figure 3A). Several other residues of the insert region anchor helix α A by making additional DNA contacts: Arg-555 hydrogen bonds to T6' and T7; and the side chains of Lys-538, Arg-540, and Asn-541 interact with the phosphate backbone (Figures 2A and 2B). Mutational analysis has shown that these phosphate contacts make a substantial contribution to the strength of the NFATC1-DNA interaction (Sun et al., 1997). The overall fold of the insert region appears to be further stabilized through hydrophobic packing involving the side chains of Phe-491, Ile-544, and Ile-553. Importantly, folding of the insert region results in the ordering of Glu-545 and Thr-551, residues that are known to participate in cooperative binding with AP-1 to DNA, but not in DNA binding by NFATC1 alone (Sun et al., 1997). Thus, induced folding processes involving multiple independent segments of the protein not only create the DNA-binding surface of NFATC1-DBD*, but also generate a template for the residues that establish cooperative contacts with partner proteins.

The Orientation of the Ig Domain on DNA Is Remodeled through Cooperative Interactions with AP-1

In addition to induced folding, transcription factors can experience other forms of induced structural remodeling upon association with other macromolecules. For example, the TATA box-binding protein (TBP) has been found to undergo twisting of one DNA-binding domain relative to the other upon interaction with DNA and TFIIB (Kim et al., 1993a; Kim et al., 1993b; Nikolov et al., 1995). The observation that NFAT and AP-1 cooperate with one

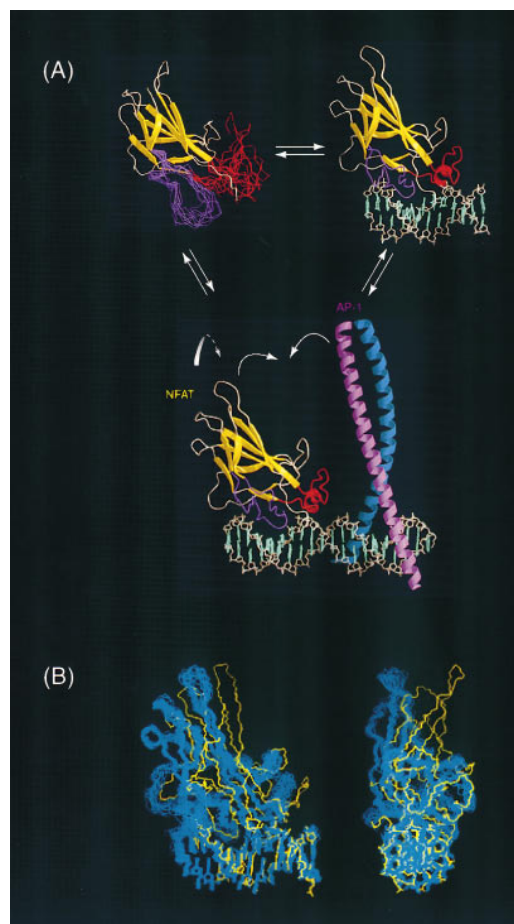


Figure 5. Induced Structural Changes Accompanying Assembly of the Ternary NFAT/AP-1/DNA Complex

(A) Top left: solution structure of NFATC1-DBD (Wolfe et al., 1997), illustrating the disorder in the DNA recognition loop (β A-B loop, magenta) and insert region (β G'-H loop, red) by the family of calculated NMR structures for those segments of the protein.

Top right: solution structure of the NFATC1-DBD* binary complex, in which the DNA recognition loop and insert region now adopt ordered structures, including a short α helix.

Lower middle: rigid-body model constructed from the solution structure of the NFATC1-DBD*/DNA complex and the X-ray structure of the AP-1 bZIP domain (Glover and Harrison, 1994), oriented as shown by affinity cleavage experiments (Chen et al., 1995). Arrows illustrate the movements of the NFAT Ig domain and AP-1 bZIP, which are necessary to position the two proteins as they are observed in the X-ray structure of the ternary NFATC2/AP-1/DNA complex (Chen et al., 1998).

(B) Overlay of C α traces of the NFATC1-DBD*/DNA solution structure (blue) with the corresponding portion of the NFATC2/AP-1/DNA X-ray structure (yellow) (Chen et al., 1998), made by least-square superposition of the DNA.

Left: view perpendicular to the long axis of the DNA (the AP-1 binding site would be to the right in ARRE2).

Right: view along the long axis of DNA (with the AP-1 binding site in ARRE2 located in front).

another on DNA through protein-protein contacts (Chen et al., 1995; Peterson et al., 1996; Sun et al., 1997) raised the question of whether some form of domain remodeling occurs in going from the binary to ternary NFAT complexes (Figure 5A). The availability of structures representing binary and ternary complexes of NFAT with

Table 2. Intermolecular Protein–DNA NOEs Identified in the Solution NFATC1–DBD*/DNA Complex that Are Incompatible with the Ternary NFATC2/AP-1/DNA Complex

Protein	DNA	Distance (H–H) in Binary Complex	Distance (H–H) Predicted from Ternary Complex	Distance (N–C) in Binary Complex	Distance (N–C) in Ternary Complex
εNH (Arg555)	H2 (A6)	4.0 ± 0.2 Å	7.3 Å	6.0 ± 0.2 Å	9.0 Å
εNH [‡] (Lys538)	CH ₃ (T3')	4.0 ± 0.4 Å	7.6 Å	5.2 ± 0.4 Å	8.9 Å
εNH [‡] (Lys538)	CH ₃ (T4')	2.8 ± 0.3 Å	6.7 Å	3.7 ± 0.4 Å	7.5 Å
εNH [‡] (Lys538)	H2'' (T5')	3.5 ± 0.4 Å	5.0 Å	4.7 ± 0.4 Å	5.4 Å
NH (Gly449)	H2'/H2'' [G(–2)]	3.5 ± 0.5 Å	5.6 Å	4.8 ± 0.5 Å	5.8 Å
NH (Gly449)	H8 [A(–1)] or C6 [T(–1) in ternary complex]	4.0 ± 0.5 Å	7.1 Å	5.0 ± 0.5 Å	7.6 Å

DNA alone (this work) and AP-1/DNA (Chen et al., 1998), respectively, allows this issue to be addressed. The orientations of the core DNA-binding domain with respect to DNA in both structures were compared by least-square superposition of the DNA (Figure 5B). The orientation of the core Ig domain of NFAT in the family of binary complex structures was found to differ from that in the ternary complex structure (Chen et al., 1998) by a 20°–24° rotation along the DNA long axis and 10°–13° pivot perpendicular to it (Figure 5B). However, because NMR spectroscopy generates a family of structures on the basis of multiple local interactions, one must be cautious in using it to deduce global features such as domain orientation. Thus, we analyzed the NMR data for interproton distance relationships that could differentiate the orientations observed in the binary and ternary complexes. Of the 56 intermolecular NOEs identified, 6 involving three different residues (Gly-449, Lys-538, and Arg-555) were found to be incompatible with the domain orientation in the ternary complex structure but compatible with that in the binary structure (Table 2). The most marked single distinction between the two orientations involves Arg-555, which projects from the insert region to contact bases of the minor groove on the 3'-end of the recognition site. In the ternary complex structure, the residue corresponding to Arg-555 (Arg-537; Chen et al., 1998) fully extends its side chain guanidinium group to contact the carbonyl of T8. By contrast, we observed NOEs between the ε-NH of Arg-555, and H2 of A6 and H4' of T6', which clearly position the Arg-555 guanidinium group within hydrogen bonding distance of T6' and T7 in the minor groove; these NOE distance constraints place Arg-555 out of reach of T8, when the Ig domain adopts the orientation observed in the binary solution structure. Importantly, the assignments of the relevant Arg-555-A6 NOE cross-peaks were confirmed via NMR experiments employing amino acid-specific labeling and positional deuteration of the protein and DNA, respectively. In addition to protein–DNA contacts unique to the binary complex that are directly supported by NOE constraints, several others can be inferred from the family of calculated NMR structures: (1) the side chain ammonium group of Lys-452 appears within hydrogen bonding distance of the G1pA(–1) backbone phosphate, and (2) the amide N-H of Ser 542 is within hydrogen bonding distance of T4'pT5'. These data provide a consistent body of evidence indicating that the orientation of the NFAT Ig domain adopts distinct orientations in the binary and ternary complexes.

What causes the NFAT Ig domain to be oriented differently in the binary and ternary complexes? One possibility is that it results from the alteration of DNA contacts accompanying mutation of His-441 to Arg. Although we cannot rigorously exclude this scenario, it seems unlikely in light of the fact that the mutation causes only modest, local changes in the conformation of the DNA recognition loop. Furthermore, with the exception of Gly-449, most of the favorable contacts unique to the binary complex bear no discernible structural dependence upon residue 448. Thus, we favor the notion that the domain orientation observed in the NFATC1–DBD*/DNA solution structure represents the energetically preferred one for a binary NFAT/DNA complex. This orientation is, however, not optimal for the establishment of cooperative protein–protein contacts with AP-1. Thus, by reorienting, NFAT is able to gain energetically favorable interactions with the AP-1 protein at the expense of some DNA contacts.

Implications for Enhanceosome Assembly

The comparison of the binary solution structure of NFAT (this work) with the X-ray structure of the ternary complex (Chen et al., 1998) thus suggests that whole-domain structural remodeling facilitates the cooperative assembly of a higher order transcriptional complex. It is now recognized that the generation of a transcriptional response in eukaryotic cells requires the cooperative promoter assembly of a particle known as an enhanceosome, which may contain a dozen or more individual DNA-binding subunits (Thanos and Maniatis, 1995; Kim and Maniatis, 1997). Most if not all of these subunits participate in enhanceosome assembly on multiple promoters, amongst which there is great variation in physical location and relationship of cooperating protein partners. Given such stereochemical diversity in enhanceosome assembly, the requirement that these proteins be capable of physically contacting each other while remaining anchored to DNA imposes a formidable geometric challenge. Whole-domain structural remodeling serves to decrease the geometric precision required for cooperative interactions on DNA and may thus be generally associated with the process of transcriptional activation in eukaryotic cells.

Implications for Discovery of Novel Immunosuppressive Agents

The potent NFAT-mediated immunosuppressive effects of FK506 and cyclosporin A, together with the pronounced lymphoid defects observed in mice bearing a

targeted disruption of the *NFATC1* gene, suggest that the NFATC1 protein is a valid target for the development of novel drugs to treat organ transplant rejection. One avenue of pursuit along these lines would be to develop agents that antagonize formation of the ternary NFAT/bZIP/DNA complex by binding to the binary NFAT/DNA complex. The solution structure reported here thus represents a direct target for drug discovery. In particular, the availability of complete resonance assignments for the binary NFATC1-DBD*/DNA complex enables direct screening of this complex against compound libraries using NMR-based methods such as SAR-by-NMR (Shuker et al., 1996).

Experimental Procedures

Overexpression and Purification of NFATC1-DBD*

An *E. coli* overexpression system for NFATC1-DBD* was generated by site-directed mutation of His 441 to Arg in the reported NFATC1-DBD expression construct (Wolfe et al., 1997). NFATC1-DBD* comprises residues 416–591 of human His441Arg NFATC1 fused to an N-terminal Met-Lys dipeptide. Uniformly ^{15}N , ^{13}C -labeled, ^{15}N -labeled, and ^{14}N -reverse labeled proteins were expressed and purified as described (Wolfe et al., 1997). Perdeuterated, ^{15}N -labeled NFATC1-DBD* was expressed in minimal media prepared using 99.9 atom% D_2O and d_3 -sodium acetate as sole carbon source. A uniformly ^{13}C , ^{15}N -labeled and fractionally deuterated protein sample was generated by overproduction in growth media prepared with 70 atom% D_2O . A sample of NFATC1-DBD containing only Arg residues labeled with ^{13}C and ^{15}N was obtained by overproduction in M9 minimal media supplemented with 100 mg/liter ^{13}C , ^{15}N -labeled Arg (Cambridge Isotopes). Fully deuterated NFATC1-DBD* containing non-deuterated Tyr and Phe residues was produced by expression in M9 minimal media (99.9 atom% D_2O) supplemented with 100 mg/liter Phe and Tyr. The protein concentration was quantified by UV spectrophotometry, using $\epsilon_{278\text{nm}} = 11,200 \text{ l mol}^{-1}\text{cm}^{-1}$.

The hairpin 12-mer duplex used in these studies had the sequence 5'-CGAGGAAAATTG-HEG-CAATTCCTCG-3', in which HEG represents a hexaethyleneglycol linker, which stabilizes duplex DNA without altering its structure (Altmann et al., 1995). It was synthesized by standard phosphoramidite chemistry, purified by denaturing gel electrophoresis, and quantified by UV spectrophotometry.

The NFATC1-DBD*/DNA complex was formed by mixing equimolar ratios of protein and DNA, allowing the mixture to equilibrate for 1 hr at room temperature, then exchanging into NMR buffer (25 mM deuterated Tris-acetate and 5 mM deuterated dithiothreitol [Cambridge Isotopes], [pH 6.5], 200 mM KCl) by centrifugal dialysis (Centricon).

Electrophoretic Mobility Shift Assays (EMSAs)

The recombinant NFATC1 C-terminal domain (residues 415–710) was expressed as a C-terminal His₆-fusion protein and purified as described (Sun et al., 1997). Recombinant c-Jun (247–340) and c-Fos (118–211) bZIP fragments were expressed and quantified as described (Peterson et al., 1996). Protein-DNA complexes studied by EMSA (6% native polyacrylamide [Protogel, National Diagnostics]) were formed by incubation at room temperature for 1 hr with 100 pM 5'-end ^{32}P -labeled DNA probe in 20 μl of binding buffer (16 mM HEPES-KOH [pH 7.5], 60 mM KCl, 30 mM NaCl, 10% glycerol, 1 mM dithiothreitol, 10 $\mu\text{g/ml}$ BSA, 5 $\mu\text{g/ml}$ poly dI-dC). Bands representing free and bound probes were quantified using a Fuji phosphorimager.

NMR Spectroscopy

NMR experiments were carried out at 27°C on Varian Unity Plus 750 MHz, Varian Inova 500 MHz, and Bruker DMX 500 MHz NMR spectrometers, all equipped with triple resonance probes. Assignments for the backbone ^1H , ^{13}C , and ^{15}N chemical shifts were obtained through 3D HNCA and HN(CO)CA on a 70% perdeuterated, ^{13}C , ^{15}N -labeled sample. These experiments, together with the amino

acid type-specific assignments (Shortle, 1994) derived from $^1\text{H}/^{15}\text{N}$ -HSQC measurements on ^{14}N -reverse labeled NFATC1-DBD* samples, allowed the sequential assignment of 162 out of 167 nonproline residues. Stereospecific methyl assignments of 7/12 valines and 7/10 leucines were directly carried over from the assignments of unliganded NFATC1-DBD (Wolfe et al., 1997). Slowly exchanging amide protons were identified through a time series of $^1\text{H}/^{15}\text{N}$ -HSQC spectra recorded after dissolving the lyophilized H_2O NMR sample into D_2O . NOE constraints for structural calculations were obtained from the following experiments: ^{15}N -separated NOESY (mixing time $\tau = 60$ ms) with a ^{15}N -labeled sample; ^{13}C -separated NOESY ($\tau = 60$ ms) with a 70% deuterated, ^{15}N , ^{13}C -labeled sample; and ^{13}C -separated NOESY ($\tau = 80$ ms) with a ^{13}C , ^{15}N -labeled sample. DNA resonances were assigned from a homonuclear $^1\text{H}/^1\text{H}$ NOESY spectrum ($\tau = 80$ ms) in D_2O using unlabeled DNA and a perdeuterated, ^{15}N -labeled protein sample. Constraints for the protein-DNA interface were derived from ^{15}N -separated NOESY ($\tau = 80$ or 120 ms) and $^1\text{H}/^1\text{H}$ NOESY spectra on a perdeuterated, ^{15}N -labeled protein sample; an aromatic region ^{13}C -edited NOESY spectrum ($\tau = 80$ ms) on a 70% deuterated, ^{13}C , ^{15}N -labeled sample; and a $^1\text{H}/^1\text{H}$ NOESY spectrum ($\tau = 60$ ms) with a fully deuterated sample containing nondeuterated Tyr and Phe residues, recorded in D_2O . Interfacial contacts made by Arg residues were assigned and distances determined by ^{15}N -separated NOESY spectra ($\tau = 80$ ms) using a fully deuterated sample selectively U- ^{13}C , ^{15}N -labeled on (nondeuterated) Arg residues. The minor groove contact involving Arg-555 was confirmed by selective loss of its cross-peak to A6 upon site-specific deuteration of the 2-positions of A4–6 (details to be reported elsewhere).

Structural Calculations

Interproton distance constraints were derived from NOESY cross-peak volumes, which were autocalibrated using CALIBA (Güntert et al., 1991). Slowly exchanging amide protons were included as hydrogen bond constraints. Hydrogen bond constraints within the DNA were used to maintain base pairing (for GC base pairs, $r_{\text{G(N1)-C(N3)}} = 2.95 \pm 0.1 \text{ \AA}$; $r_{\text{G(H1)-C(N3)}} = 1.95 \pm 0.1 \text{ \AA}$; $r_{\text{G(O6)-C(N4)}} = 2.91 \pm 0.1 \text{ \AA}$; $r_{\text{G(O6)-C(H41)}} = 1.91 \pm 0.1 \text{ \AA}$; $r_{\text{G(N2)-C(O2)}} = 2.86 \pm 0.1 \text{ \AA}$; $r_{\text{G(H21)-C(O2)}} = 1.86 \pm 0.1 \text{ \AA}$; for AT base pairs, $r_{\text{A(N1)-T(N3)}} = 2.82 \pm 0.1 \text{ \AA}$; $r_{\text{A(N1)-T(H3)}} = 1.82 \pm 0.1 \text{ \AA}$; $r_{\text{A(N6)-T(O4)}} = 2.95 \pm 0.1 \text{ \AA}$; $r_{\text{A(H61)-T(O4)}} = 1.95 \pm 0.1 \text{ \AA}$; Saenger, 1984; Brünger, 1992). Dihedral angle constraints were generated by HABAS (Güntert et al., 1991) based on chemical shift index (CSI) and NOE patterns. Initial structures were generated using the program DYANA (Güntert et al., 1997) starting from random conformations of protein and B-form DNA. Of the 100 total calculated structures, the 30 best were subjected to molecular dynamics using the simulated annealing procedure in X-PLOR (Brünger, 1992). Loose hydrogen bond restraints (lower bound, 2.8 \AA ; upper bound, 4.0 \AA) involving arginine-G contacts between the guanidinium N_η atoms and O6/N7 of guanines were introduced during the final stage of refinements. This routine produced 18 final structures with no NOE violations $>0.4 \text{ \AA}$ and no dihedral angle violations $>5.0^\circ$. The statistics provided in Table 1 represent all 18 final calculated structures, which are displayed in Figure 2A.

Acknowledgments

We thank Gerald Crabtree for providing the *NFATC1* cDNA, sharing unpublished data, and discussing signal integration by NFAT. We thank Scot Wolfe for numerous discussions during the course of this investigation. We are grateful to Lin Chen and Steve Harrison for sharing their X-ray structural information on the ternary NFATC2/AP-1 bZIP/DNA complex, and especially to Lin Chen for extensive discussions on the similarities and differences observed in the binary and ternary complexes, which were determined independently. We also thank Tom Wintner and Hideo Tomozane for providing the C2-deuterated dA, and hexaethylene glycol linker phosphoramidites. This work was supported by grants from the NIH (P01 GM47467) and Hoffmann-La Roche Institute of Chemistry and Medicine. The NMR spectrometers used in this work were purchased with funding provided by Harvard Medical School, NSF, NIH, and Giovanni Armenisi Foundation. V. D. was partially supported by

postdoctoral fellowships from NSF and EMBO; P. Z. is an Eli Lilly Fellow.

Received January 27, 1998; revised February 19, 1998.

References

- Altmann, S., Labhardt, A.M., Bur, D., Lehmann, C., Bannwarth, W., Billeter, M., Wüthrich, K., and Leupin, W. (1995). NMR studies of DNA duplexes singly cross-linked by different synthetic linkers. *Nucleic Acids Res.* **23**, 4827–4835.
- Beals, C.R., Clipstone, N.A., Ho, S.N., and Crabtree, G.R. (1997). Nuclear localization of NF-ATc by a calcineurin-dependent, cyclosporin-sensitive intramolecular interaction. *Genes Dev.* **11**, 824–834.
- Bork, P., Holm, L., and Sander, C. (1994). The immunoglobulin fold: structural classification, sequence patterns and common core. *J. Mol. Biol.* **242**, 309–320.
- Brünger, A.T. (1992). X-PLOR 3.1 Manual (New Haven, CT: Yale University Press).
- Chen, L., Oakley, M.G., Glover, J.N.M., Jain, J., Dervan, P.B., Hogan, P.G., Rao, A., and Verdine, G.L. (1995). Only one of the two DNA-bound orientations of AP-1 found in solution cooperates with NFATp. *Curr. Biol.* **5**, 882–889.
- Chen, L., Glover, J.N.M., Hogan, P.G., Rao, A. and Harrison, S.C. (1998). X-ray structure of the NFATp/AP-1/DNA complex. *Nature*, in press.
- Crabtree, G.R., and Clipstone, N.A. (1994). Signal transmission between the plasma membrane and the nucleus of T lymphocytes. *Annu. Rev. Biochem.* **63**, 1045–1083.
- Ferre-D'Amare, A.R., Prendergast, G.C., Ziff, E.B., Burley, S.K. (1993). Recognition by Max of its cognate DNA through a dimeric b/HLH/Z domain. *Nature* **363**, 38–45.
- Fisher, D.E., Parent, L.A., and Sharp, P.A. (1993). High affinity DNA-binding Myc analogs: recognition by an α helix. *Cell* **72**, 467–476.
- Flanagan, W.M., Corthésy, B., Bram, R.J., and Crabtree, G.R. (1991). Nuclear association of a T-cell transcription factor blocked by FK-506 and cyclosporin A. *Nature* **352**, 803–807.
- Ghosh, G., Van Duyane, G.D., Ghosh, S., and Sigler, P.B. (1995). Structure of NF- κ B p50 homodimer bound to a κ B site. *Nature* **373**, 303–310.
- Glover, J.N.M., and Harrison, S.C. (1994). The crystal structure of the heterodimeric bZip transcription factor cFos:cJun bound to DNA. *Nature* **373**, 257–261.
- Güntert, P., Braun, W., and Wüthrich, K. (1991). Efficient computation of the three-dimensional protein structures in solution from nuclear magnetic resonance data using the program DIANA and the supporting programs CALIBA, HABAS and GLOMSA. *J. Mol. Biol.* **217**, 517–530.
- Güntert, P., Mumenthaler, C., and Wüthrich, K. (1997). Torsion angle dynamics for NMR structure calculation with the new program DYANA. *J. Mol. Biol.* **273**, 283–298.
- Hodge, M.R., Ranger, A.M., de la Brousse, F.C., Hoey, T., Grusby, M., and Glimcher, L.H. (1996). Hyperproliferation and dysregulation of IL-4 expression in NF-ATp-deficient mice. *Immunity* **4**, 397–405.
- Hoey, T., Sun, Y.-L., Williamson, K., and Xu, X. (1995). Isolation of two new members of the NF-AT gene family and functional characterization of the NF-AT proteins. *Immunity* **2**, 461–472.
- Jain, J., McCaffrey, P.G., Valge-Archer, V.E., and Rao, A. (1992). Nuclear factor of activated T cells contains Fos and Jun. *Nature* **356**, 801–804.
- Jain, J., Miner, Z., and Rao, A. (1993). Analysis of the preexisting and nuclear forms of nuclear factor of activated T cells. *J. Immunol.* **151**, 837–848.
- Jain, J., Burgeon, E., Badalian, T.M., Hogan, P.G., and Rao A. (1995). A similar DNA-binding motif in NFAT family proteins and the rel homology region. *J. Biol. Chem.* **270**, 4138–4145.
- Kim, T.K. and Maniatis, T. (1997). The mechanism of transcriptional synergy of an in vitro assembled interferon- β enhanceosome. *Mol. Cell* **1**, 119–129.
- Kim, J.L., Nikolov, D.B., and Burley, S.K. (1993a). Co-crystal structure of TBP recognizing the minor groove of a TATA element. *Nature* **365**, 520–527.
- Kim, Y., Geiger, J.H., Hahn, S., and Sigler, P.B. (1993b). Crystal structure of a yeast TBP/TATA-box complex. *Nature* **365**, 512–520.
- Laskowski, R.A., Rullmann, J.A., MacArthur, M.W., Kaptein, R., and Thornton, J.M.J. (1996). AQUA and PROCHECK-NMR: programs for checking the quality of protein structures solved by NMR. *J. Biomol. NMR*, **8**, 477–486.
- Liu, J., Farmer, J.D., Jr., Lane, W.S., Friedman, J., Weissman, I., and Schreiber, S.L. (1991). Calcineurin is a common target of cyclophilin-cyclosporin A and FKBP-FK506 complexes. *Cell* **66**, 1–9.
- Luo, C., Shaw, K.T.Y., Raghavan, A., Aramburu, J., Garcia-Cozar, F., Perrino, B.A., Hogan, P.G., and Rao, A. (1996). Interaction of calcineurin with a domain of the transcription factor NFAT1 that controls nuclear import. *Proc. Natl. Acad. Sci. USA* **93**, 8907–12.
- Müller, C.W., Rey, F.A., Sodeoka, M., Verdine, G.L., and Harrison, S.C. (1995). Structure of the NF- κ B p50 homodimer bound to DNA. *Nature* **373**, 301–317.
- Nikolov, D.B., Chen, H., Halay, E.D., Usheva, A.A., Hisatake, K., Lee, D.K., Roeder, R.G., and Burley, S.K. (1995). Crystal structure of a TFIIB-TBP-TATA-element ternary complex. *Nature* **377**, 119–128.
- Patel, L., Abate, L., and Curran, T. (1990). Altered protein conformation on DNA binding by Fos and Jun. *Nature* **347**, 572–575.
- Peterson, B.R., Sun, L.J., and Verdine, G.L. (1996). A critical arginine residue mediates cooperativity in the contact interface between NFAT and AP-1. *Proc. Natl. Acad. Sci. USA* **93**, 13671–13676.
- Rao, A. (1994). NFATp: a transcription factor required for the coordinate induction of several cytokine genes. *Immunol. Today* **15**, 274–281.
- Rao, A., Luo, C., and Hogan, P.G. (1997). Transcription factors of the NFAT family: regulation and function. *Annu. Rev. Immunol.* **15**, 707–747.
- Saenger, W. (1984). Principles of Nucleic Acid Structure (New York: Springer-Verlag).
- Shibasaki, F., Price, E.R., Milan, D., and McKeon, F. (1996). Role of kinases and the phosphatase calcineurin in the nuclear shuttling of transcription factor NF-AT4. *Nature* **332**, 370–373.
- Shortle, D. (1994). Assignment of amino acid type in ^1H - ^{15}N correlation spectra by labeling with ^{14}N amino acids. *J. Mag. Res. B* **105**, 88–90.
- Shuker, S.B., Hajduk, P.J., Meadows, R.P., Fesik, S.W. (1996). Discovering high-affinity ligands for proteins: SAR by NMR. *Science* **274**, 1531–1534.
- Spolar, R.S., and Record, M.T., Jr. (1994). Coupling of local folding to site-specific binding of proteins to DNA. *Science* **263**, 777–784.
- Sun, L.J., Peterson, B.R., and Verdine, G.L. (1997). Dual role of the NFAT insert region in DNA recognition and cooperative contact to AP-1. *Proc. Natl. Acad. Sci. USA* **94**, 4919–4924.
- Thanos, D., and Maniatis, T. (1995). Virus induction of human *IFN β* gene expression requires the assembly of an enhanceosome. *Cell* **83**, 1091–1100.
- Weiss, M.A., Ellenberger, T., Wobbe, C.R., Lee, J.P., Harrison, S.C., and Struhl, K. (1990). Folding transition in the DNA-binding domain of GCN4 on specific binding to DNA. *Nature* **347**, 575–578.
- Wolfe, S.A. (1996). Structural studies on the DNA Binding Domain of Human NFATC. PhD thesis, Harvard University, Cambridge, Massachusetts.
- Wolfe, S.A., Zhou, P., Dötsch, V., Chen, L., You, A., Ho, S.N., Crabtree, G.R., Wagner, G., and Verdine, G.L. (1997). An unusual Rel-like architecture in the DNA-binding domain of NFATc. *Nature* **385**, 172–176.
- Woodrow, M.A., Rayter, S., Downward, J., and Cantrell, D.A. (1993). p21^{ras} function is important for T cell antigen receptor and protein kinase C regulation of nuclear factor of activated T cells. *J. Immunol.* **150**, 3853–3861.
- Xanthoudakis, S., Viola, J.P.B., Shaw, K.T.Y., Luo C., Wallace, J.D., Bozza, P.T., Luk, D.C., Curran, T., and Rao, A. (1996). An enhanced immune response in mice lacking the transcription factor NFAT1. *Science* **272**, 892–895.